Physica E 42 (2009) 124–131

Contents lists available at ScienceDirect

Physica E

journal homepage: www.elsevier.com/locate/physe

Secondary electron emission from single-walled carbon nanotubes

M.K. Alam, S.P. Eslami, A. Nojeh *

Department of Electrical & Computer Engineering, University of British Columbia, Vancouver, Canada, BC V6T 1Z4

ARTICLE INFO

Article history:
Received 12 June 2009
Received in revised form
10 September 2009
Accepted 17 September 2009
Available online 26 September 2009

PACS:
78.70.−g
73.22.−f
61.48.De

Keywords:
Secondary emission
First-principles simulations
Nanotubes
Electron microscopy
Energy loss
Charge–matter interaction

ABSTRACT

To study secondary electron emission from single-walled carbon nanotubes and their visibility in scanning electron microscopy, their electronic structure is investigated in the presence of external electrons using first-principles calculations. By using the obtained nanotube charge density distribution, the energy loss of primary electrons as they pass through the electronic cloud of nanotube orbitals is estimated and it is shown that there could be enough energy transfer via inelastic scattering to allow the emission of secondaries. In addition, it is observed that the primary electron causes a major upward shift in occupied energy levels of the nanotube, effectively reducing the ionization energy and significantly increasing the secondary emission probability. It is also seen that if the nanotube has enough time to relax in response to the electric field of the primary electron, its ionization energy is lowered even more, further enhancing the secondary emission.

1. Introduction

Carbon nanotubes are hollow cylindrical structures of carbon with nanoscale diameters. Due to their extraordinary mechanical and electrical properties, nanotubes have potential applications in a variety of areas such as light-weight, high-strength composites, improved hydrogen storage media, new devices for future-generation electronics and air pollution filters. They have also been shown to enable robust, stable, low-voltage and high-brightness electron emitters [1,2]. High-quality electron emitters are in demand in various applications such as flat-panel displays, vacuum nanoelectronics, free-electron analog to digital converters, electron microscopes and patterning systems [1]. Scanning electron microscopy (SEM) can be used to image and inspect a wide variety of micro- and nano-structures such as individual and ropes of single-walled nanotubes (SWNTs) [2], highly oriented forests of multi-walled nanotubes (MWNTs) [3], for nanowelding [4] or to study the interaction of electron beams with various materials, such as in electron-stimulated field-emission from nanotubes [5,6]. Several experimental studies have been carried out on the SEM imaging of SWNTs [7–10]. Yet, it is quite surprising that small and hollow structures like nanotubes are so readily visible in an SEM. Recently, Finnie et al. [11] demonstrated imaging of suspended nanotubes by scanning electron microscopy based on the charging of nanotubes due to secondary electron emission. But, to the best of our knowledge, no direct explanation has yet been given for the secondary emission mechanism itself in nanotubes. Due to the extremely small interaction area of the nanotube with the electron beam that does not provide much possibility for scattering high-energy electrons, this visibility cannot be explained by traditional beam-bulk multiscattering models. We have previously investigated the emission of electrons from the tip of a nanotube under external bias and in the presence of primary electrons. Using first-principles calculations, we observed that a primary electron entering the nanotube tip region raises the orbital energies and makes their occupying electrons more susceptible to tunneling out of the nanotube [6]. In normal SEM imaging, secondary emission from the sidewall of a nanotube, without a notable external field must be studied, which is the subject of the present work.

2. The model

Existing Monte-Carlo models for SEM are based on the multiple scatterings of primary electrons with many atoms in a solid [12]. A nanotube cannot be adequately modeled with these methods as it is a single layer of atoms with a very small

* Corresponding author.
E-mail address: anojeh@ece.ubc.ca (A. Nojeh).

1386-9477/$ - see front matter © 2009 Elsevier B.V. All rights reserved.
doi:10.1016/j.physe.2009.09.012

interaction area, which means that there is a low likelihood of scattering events with the primary beam of the SEM. An alternative approach is to directly study the effect of primary electrons on the electronic structure of the nanotube to investigate how it may lead to secondary emission. Semi-empirical or continuum modeling of SWNTs are computationally efficient, but may not capture all the nanoscale effects accurately. Therefore, here we use first-principles quantum mechanical modeling to explore the interaction of an electron beam with SWNTs. Small sections of nanotubes were modeled due to high computational cost of the first-principle calculations. Here 7½ unit cells of a (5,5) SWNT (metallic) and 4 unit cells of a (8,0) SWNT(semiconducting) were chosen as the structures to be simulated. A similar size structure has been used in several previous studies on nanotubes and has been observed to reproduce the electronic structure quite accurately [6,13,14]. The SWNTs were terminated with hydrogen atoms to avoid dangling bonds and simulated in the presence of a single electron fixed at various positions (Fig. 1(a) and (b)). It is reasonable to consider the primary beam electrons from the SEM only one at a time because under typical SEM beam current and energy conditions for nanotube imaging, electrons in the primary beam are on average several meters apart from each other. For instance, at 5 keV and 0.7 pA, there is only one electron in every 13 m of the beam length [6]. The electron was placed at five different locations from the center to the outside of the nanotube.

The Hartree–Fock (HF) method in the software package Gaussian 03 [15] was primarily used for simulations. This method, when used with an appropriate basis set such as 6-31G(d), has been observed to reproduce the occupied energy levels of such nanotube systems quite accurately, and is therefore suitable for problems involving ionization energies and electron emission [6]. This method has also been compared for density functional theory (DFT) calculations and found to be in good agreement with such problems [6].

For each nanotube, the initial atomic coordinates were generated using the software Nanotube Modeler. Before calculating the electronic structure of the nanotube in each case, one needs to find the relaxed atomic structure of the system. This 'geometry optimization' step is computationally very expensive, and it is desirable to perform it with a minimal basis set such as STO-3G, which enables much faster relaxation simulations than the more accurate 6-31G(d). We performed comparison simulations with both basis sets on a small sub-system (one unit cell of the (5,5) nanotube). The distances between various pairs of atoms and the HOMO and LUMO energy levels were compared to check whether the results provided by STO-3G would be reasonably close to those provided by 6-31G(d) (Tables 1 and 2).

In all compared cases, the difference in bond lengths was less than 0.8% and the difference in orbital energies was less than 0.5%. Moreover, our interest in this problem is in the electronic structure, and not in bond lengths themselves. Obviously a 0.8% inaccuracy in atomic coordinates would have a minimal effect in the electronic structure (of course this would not be appropriate for a problem where small changes in bond lengths and atomic coordinates are the main topic of study, such as the electromechanical actuation of carbon nanotubes [16]). Therefore, for the rest of the simulations, we used STO-3G for geometry optimization in order to have a better computational efficiency. However, the single point energy calculations after each geometry optimization step were all carried out using the 6-31G(d) basis set to preserve a higher level of accuracy. Ionization energy (from potential profiles) and electron–electron interaction depth (from charge density profile) were then estimated from the ab-initio calculations. Average energy transfer from the primary beam of the SEM to the SWNT was calculated for a typical range of primary beam energies to gain insight into the mechanism of secondary emission from SWNTs.

Table 1
Distance (in Å) between different atoms.

Atoms (arbitrarily chosen)	6-31G(d)	STO-3G	Difference (%)
C10–C26	6.95452	6.95969	−0.0789
C10–C13	2.3541	2.36724	−0.5581
C10–C24	7.34215	7.35126	−0.1241
C10–C28	7.12276	7.13985	−0.2399
C8–C11	1.50502	1.5163	−0.7494

Table 2
Energy (in Hartrees) of HOMO and LUMO.

Molecular orbitals	6-31G(d) optimized	STO-3G optimized	Difference (%)
HOMO	−0.224	−0.225	−0.4464
LUMO	0.046	0.046	0.0000

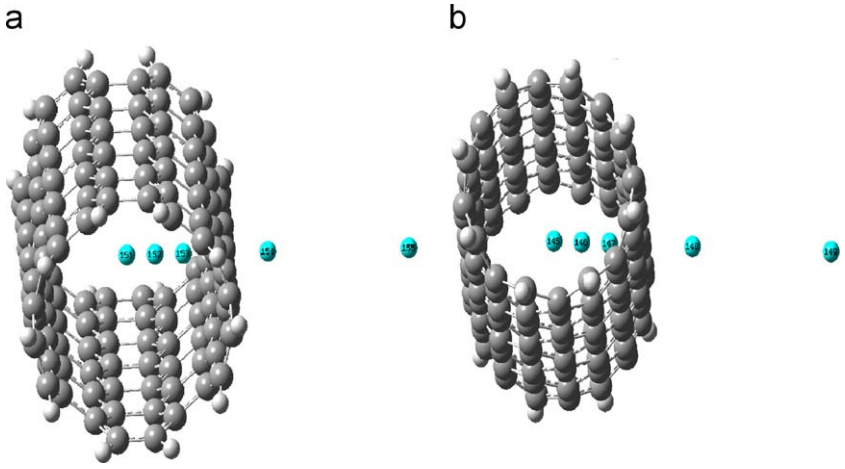

Fig. 1. (a) (5,5) SWNT with various positions of the extra electron. In each simulation, the electron is placed in one of these positions. They are located at the center, 1 Å away from the center, 2 Å away from the center, 5 Å away from the center and 10 Å away from the center. Once the electron is located 5 Å or more away from the center, it is outside of the nanotube (b) (8,0) SWNT with the same electron positions as in (a).

3. Results and discussion

In principle, the structure of the nanotube might be deformed due to the electric field of the incoming electron. However, due to the high velocity of the electron, it is not clear whether the nanotube structure will have enough time to respond and change to a new relaxed configuration that is determined by the incoming electron's field. Nonetheless, since there might still be some change in atomic coordinates due to the primary electron, we have carried out simulations on both the relaxed and non-relaxed structures in the presence of the additional electron in order to cover both ends of the spectrum of possibilities. Also, the (5,5) and (8,0) SWNTs gave generally similar results. So in this section, results for (5,5) SWNT are mainly presented.

3.1. The non-relaxed (5,5) SWNT

The results discussed below are for the case where a single extra electron was fixed at various positions and single point energy calculations were done without carrying out a relaxation (geometry optimization). First, the energy levels were calculated without any primary beam (i.e. no extra point charge in simulations). The occupied levels were all below the vacuum level, as expected. The highest occupied molecular orbital (HOMO) was at -5.1 eV. This value agrees closely with the ionization energy of the nanotube, which is known to be around 5 eV, and this further justifies our model and use of the Hartree–Fock level of theory [6]. Fig. 2 shows the Mulliken charge distribution and HOMO molecular orbital structure for the (5,5) nanotube with no background charge. The molecular orbital is evenly distributed as expected. Also the Mulliken charge diagram shows that the effect of the hydrogen termination is limited to the first ring of carbon atoms on either side (the local dipole is due to the difference in the electro-negativity of hydrogen and carbon), and that the majority of the length of the nanotube is unaffected by the edges. This further confirms that the length of the cluster is appropriate for these simulations.

Fig. 3 shows the directions along which electrostatic potential energy profiles were investigated. The purpose of analyzing the potential profiles in different directions is to provide an insight into where electrons are more likely to tunnel out or overcome the vacuum barrier of the nanotube. The directions are as follows:

x1	in the positive horizontal direction through the center of the nanotube
x2	in the positive horizontal direction two rings below the center
y1	into the page through the center of the nanotube
y2	into the page two rings below the center

Figs. 4 and 5 illustrate the potential profile with no background charge and charge at the center of the nanotube, respectively, in the four chosen directions. It can be seen that the profiles are rather similar in all these directions. The potential profiles were shifted on each figure to keep the highest occupied molecular orbital (HOMO) constant in all cases for ease of comparison. The

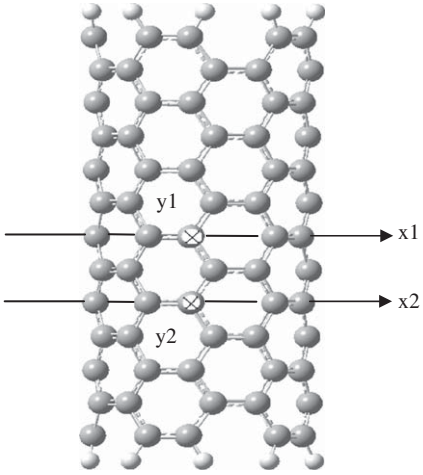

Fig. 3. Directions along which potential profiles are plotted. [x1—in the positive horizontal direction through the center of the nanotube; x2—in the positive horizontal direction two rings below the centre; y1—into the page through the center of the nanotube; and y2—into the page two rings below the center]

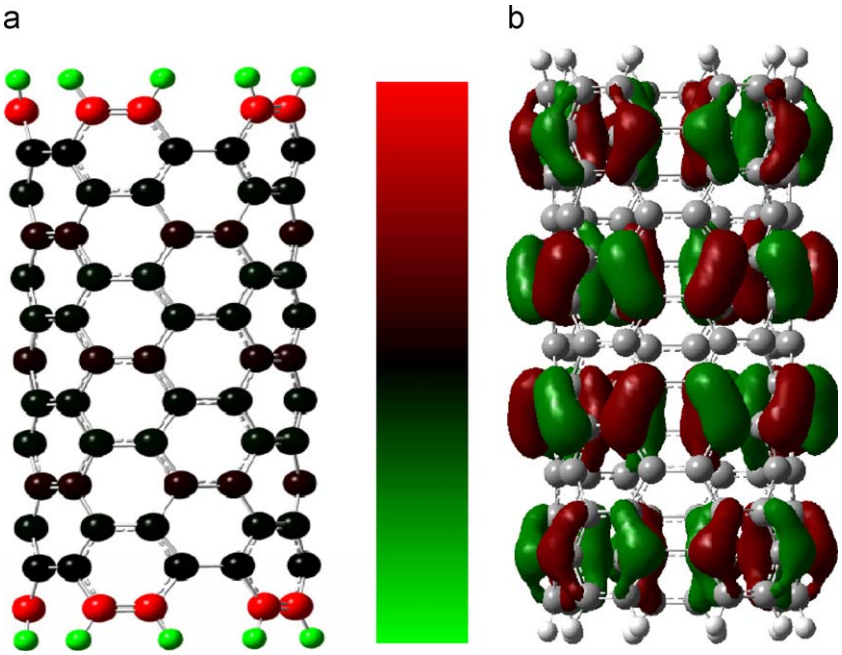

Fig. 2. (a) Mulliken charge distribution and (b) HOMO of (5,5) SWNT in the absence of charge.

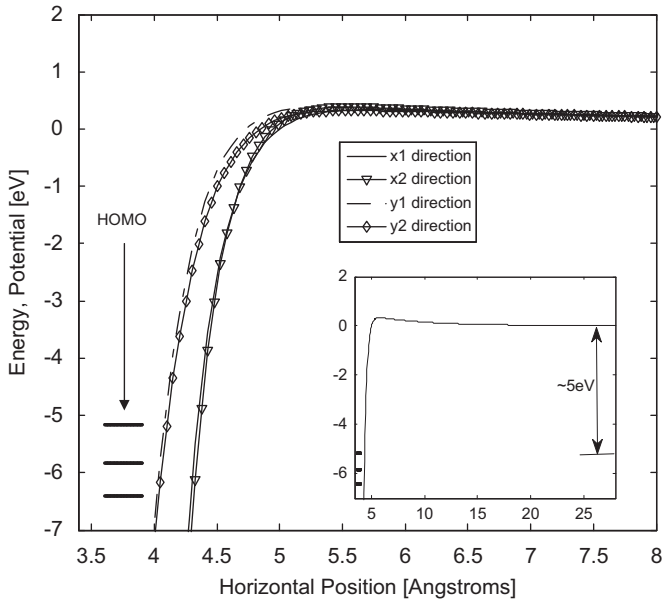

Fig. 4. Potential profiles and energy levels of (5,5) SWNT without any background charge.

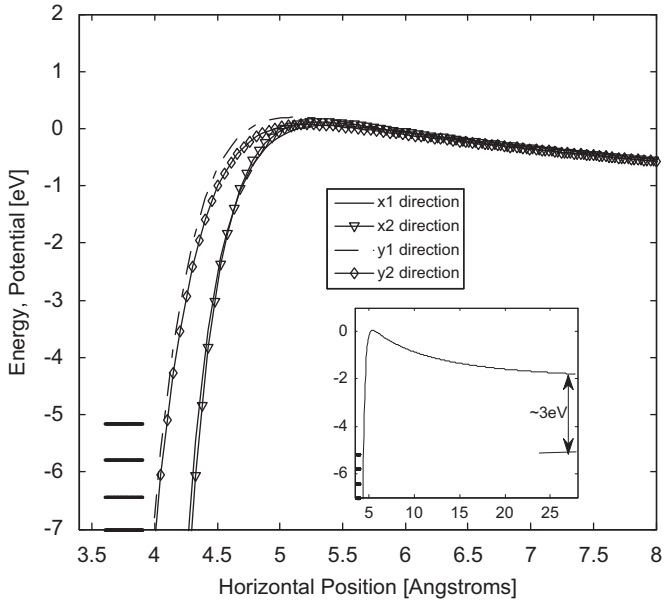

Fig. 5. Potential profiles and energy levels of (5,5) SWNT with charge at the center of the tube.

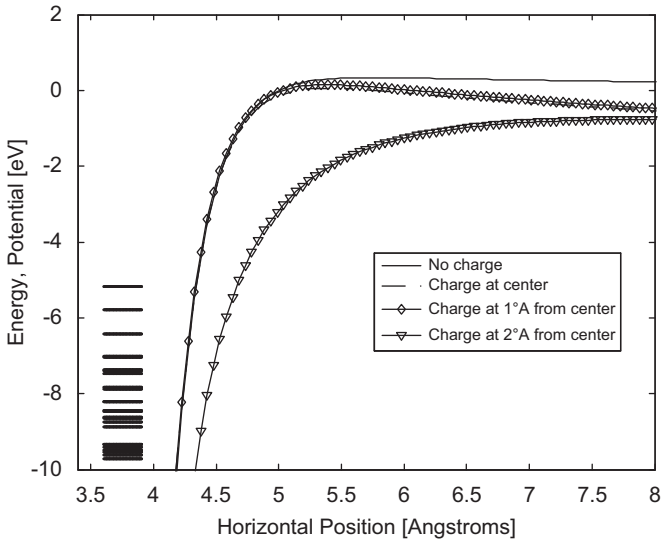

Fig. 6. Potential profiles and energy levels of (5,5) SWNT in x1 direction for various positions of electron.

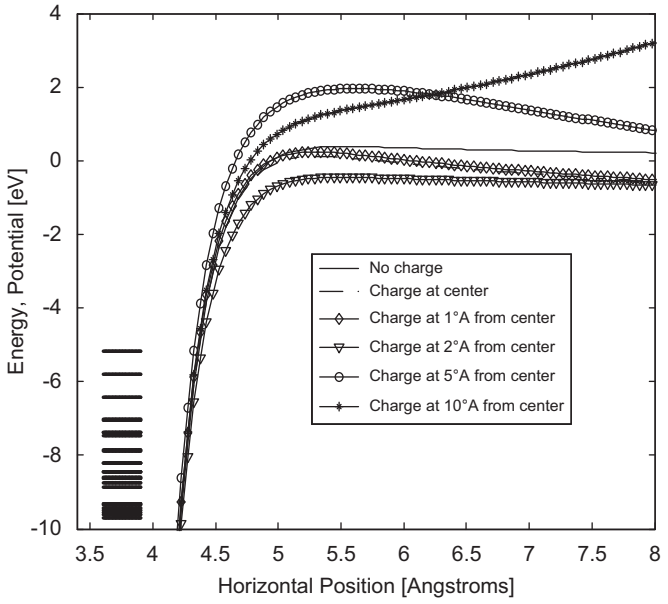

Fig. 7. Potential profiles and energy levels of (5,5) SWNT in x2 direction for various positions of electron.

insets show the potential profile over a longer distance to show the vacuum level outside the nanotube and the effective barrier heights. As can be seen in Fig. 5, due to the presence of the extra electron, the gap between HOMO and the vacuum level is lowered by more than 2 eV (Fig. 5 inset) compared to Fig. 4. Although there still exists a local potential barrier of almost 5 eV in Fig. 5, this barrier is less than 1.5 nm thick and the nanotube electrons can tunnel through it. Therefore, the ionization energy has been reduced from ~5 to ~3 eV due to the presence of the extra electron.

Figs. 6 and 7 show the potential profiles and energy levels along x1 and x2 directions, respectively for different positions of the primary electron. For the x1 direction, note that, due to the Pauli exclusion principle and coulombic interactions, the emitted secondary electron will never go through the point where the primary electron is. Therefore, on Fig. 6, we have only plotted the potential barrier for the cases where the primary electron does not stand on the way of the emitted secondary electron. As can be seen from the barrier heights and shapes in various cases, the ionization energy is smallest when the extra charge is inside the tube. In particular, when the extra charge is inside the nanotube, 2 Å from the center (relatively close to the nanotube wall), even the local barrier has been considerably lowered. Similar profiles were found for cases where the extra electron was placed at 1.5–3.0 Å from the center (not shown here). As expected there was no significant decrease in the potential barrier in the y1 and y2 directions (Figs. 8 and 9).

The observed effective decrease of ~2 eV in ionization energy due to the presence of the extra electron (representing the

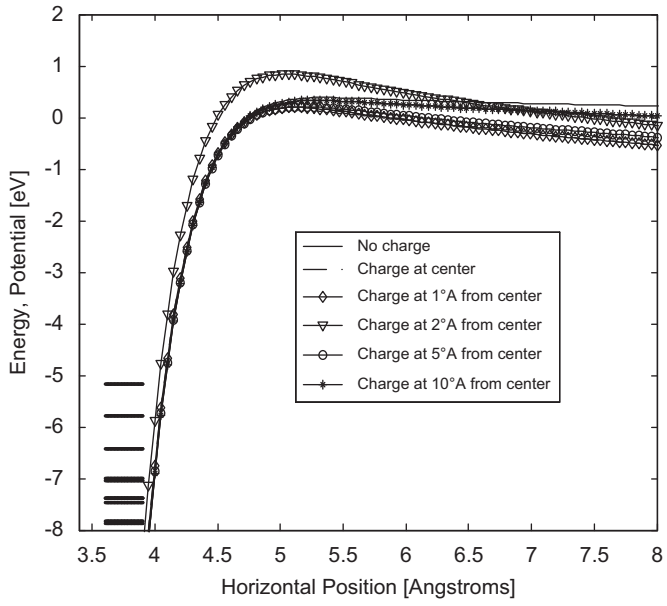

Fig. 8. Potential profiles and energy levels of (5,5) SWNT in y1 direction for various positions of electron.

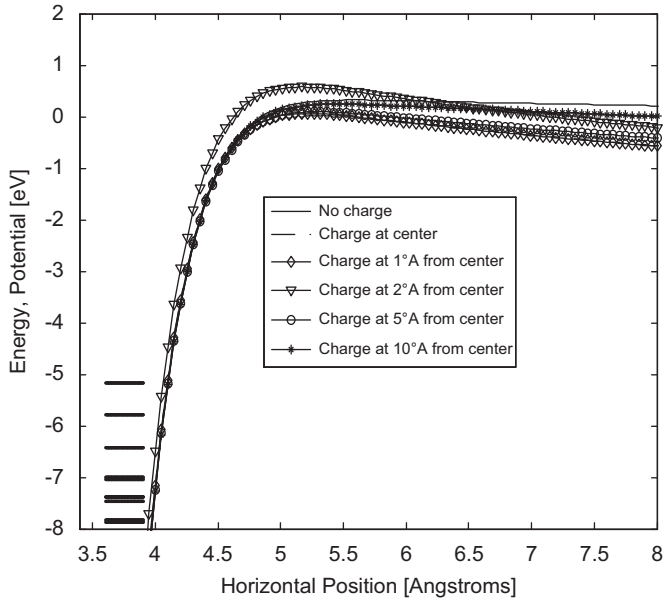

Fig. 9. Potential profiles and energy levels of (5,5) SWNT in y2 direction for various positions of electron.

primary beam) in certain locations suggests a significant increase in the emission of electrons from the nanotube, and might provide a partial explanation for secondary electron emission. A similar reduction in emission barrier happens when the nanotube is under a strong external field [17,18]. In order to quantify the effect of this decrease in ionization potential on the secondary emission current, one possibility is to look at thermionic emission (for instance, at a very low workfunction, there could be significant thermionic emission even at room temperature). The thermionic emission current density can be calculated using the the Richardson–Dushman equation:

$$J_T = AT^2 e^{(-\Phi/kT)}, \tag{1}$$

where A is the Richardson constant, k is the Boltzmann constant, T is absolute temperature and Φ is the workfunction. Eq. (1) suggests that the emission current rises dramatically (of the order 10^{25}–10^{35}) due to the workfunction lowering (to be more precise the lowering of the ionization energy in our simulations) because of the presence of an extra electron. However, the actual value of the current might still be very small (for instance, at room temperature, this leads to an increase from $\sim 10^{-70}$ to $\sim 10^{-35}$ A/m^2 in the best case). Therefore, it is doubtful that thermionic emission can provide an explanation for the observed secondary electron emission in nanotubes. Below other possibilities are investigated.

A primary electron travelling with a typical energy of 300 eV–30 keV might have both elastic scattering (due to interaction with nuclear potentials and acoustic phonons) and inelastic scattering (due to interaction with the electrons in the system). Radiation loss (Bremsstrahlung) does not lead to secondary electron emission (as the name implies this loss is associated with photon emission). For secondary emission we are interested in inelastic scattering that leads to energy transfer to nanotube electrons. This is directly related to the effective interaction volume for the primary electron and the nanotube. As mentioned previously, this volume is extremely small due to the nanoscale diameter of the nanotube. However, if the primary electron has a chance to experience multiple changes in direction due to elastic scatterings and bounce around inside the nanotube for some time, the effective interaction volume will be increased. Therefore, we first look at the likelihood of multiple elastic scattering events. The possibility of elastic scattering due to atomic potentials is determined by the elastic scattering cross-section i.e. the Mott cross-section, which can be calculated from the empirical equation given by Browning et al. [19] (also available from exact numerical calculation [20]):

$$\sigma_T = \frac{3 \times 10^{-18} Z^{1.7}}{E + 0.005 Z^{1.7} E^{1.5} + 0.0007 Z^2 / E^{0.5}} \text{ cm}^2, \tag{2}$$

where E is the incident energy and Z is the atomic number. For a carbon atom, for the energy range of primary beam mentioned above this equation gives a value in the 10^{-23}–10^{-25} m^2 range, which suggests a negligible area around an atom available for elastic scattering in a SWNT ($\sim$0.016% in the best case for a C–C distance of $\sim$1.4 Å). As a result, it is extremely unlikely that the primary electron could become "trapped" inside the nanotube through multiple elastic reflections from the inside of the nanotube wall. Therefore, we will look at the energy loss of the primary electron as it makes one pass through the nanotube, perpendicular to it.

The main energy loss mechanism for the primary electron is from electron–electron inelastic scattering, which could lead to secondary electron emission, as in the case of bulk solids. The difference is that there are no multiple scattering events in the nanotube as discussed previously. The question, then, is whether one pass through the nanotube (perpendicular to it) will allow enough energy transfer from the primary to the nanotube electrons via inelastic scattering. Under Bethe's continuous-slowing-down approximation, the empirical energy loss equation proposed by Joy and Luo [21] can be used for the estimation of average energy loss due to inelastic electron–electron collisions:

$$\frac{dE}{dx} = -785 \frac{\rho Z}{AE} \ln\left(\frac{1.166(E+tJ)}{J}\right) \text{eV/Å}, \tag{3}$$

where x is the interaction length in the travelling direction of the primary electron, ρ is the density of the target, Z is the atomic number, A is the atomic weight, E is the incident energy, J is the mean excitation potential (in the absence of a value specific to nanotubes, we used the empirical value of 78 eV for carbon [22]) and t is an empirical factor, which is 0.57 for carbon. Whether a

continuous-slowing-down approximation can be applied to the case of a primary electron passing through a nanotube is not obvious, since the electron effectively "sees" only two separate layers of atoms. Nonetheless, we used this equation to gain a first-order insight into the problem. For this the effective thickness of the nanotube determined by the extension of its electronic cloud was needed. We used the ab-initio simulation results discussed previously to plot the electron density distribution along the primary beam path (Fig. 10). An important issue to consider is that the primary electron can affect this distribution as it moves. To gain further insight, we show this distribution for various locations of the primary beam on Fig. 10. It can be seen that although the primary electron affects the electron density distribution, the total effective thickness of the nanotube obtained from this distribution is not significantly changed (less than ~5% change in the width and, therefore, in the energy loss in the worst case). The energy loss was then calculated from Eq. (3) as a function of the primary beam energy (Fig. 11). It can be seen that a low-energy primary electron (a few hundred eV) can lose up to ~40 eV during one full pass through the nanotube. This energy loss quickly decreases as the initial energy of the primary electron increases.

As we saw from the ab-initio simulations discussed earlier, the ionization energy of the nanotube is ~5 eV, and it reduces to ~3 eV when the primary electron reaches inside the nanotube. Thus, according to the energy loss results of Fig. 11, we expect secondary electrons to be generated from one of the following mechanisms:

- When the primary beam has reached around the center of the nanotube, the ionization energy of the nanotube has been reduced to around 3 eV, although a local barrier of 5 eV still remains for the secondary emission (see Fig. 5). According to Fig. 11, if the primary electron energy has been less than ~3.5 keV, the energy loss is greater than ~5 eV. If enough of this energy is transferred to a given nanotube electron, that electron can be emitted as a secondary by directly overcoming the vacuum barrier.
- If the primary energy is between 3.5 and 7.5 keV, the energy loss by the time the primary reaches the center of the nanotube is less than 5 eV, but more than 3 eV. This means, according to Fig. 5, that if this entire energy is transferred to the HOMO electron of the nanotube, that electron can be excited to a high-enough level to be able to subsequently tunnel out of the nanotube (Fig. 12).
- After the primary electron has completed a full pass and exited from the other side of the nanotube, the ionization energy has gone back to 5 eV. But according to Fig. 11, for primary beam energies of up to approximately 10 keV, there is enough energy loss to allow the emission of secondaries.
- If the energy transfer is not sufficient for any of the above to take place, but greater than the bandgap of the nanotube, that is enough for the HOMO–LUMO or any occupied–unoccupied state transition, a multiple-step process might take place (several nanotube electrons being excited to higher energy levels due to multiple primary beam electrons and all of them relaxing almost simultaneously and the sum of their energies helping another nanotube electron to overcome the vacuum barrier). Obviously, these events would occur with a very low probability, although with increased primary beam current (more primary electrons present at once) this probability might also increase.

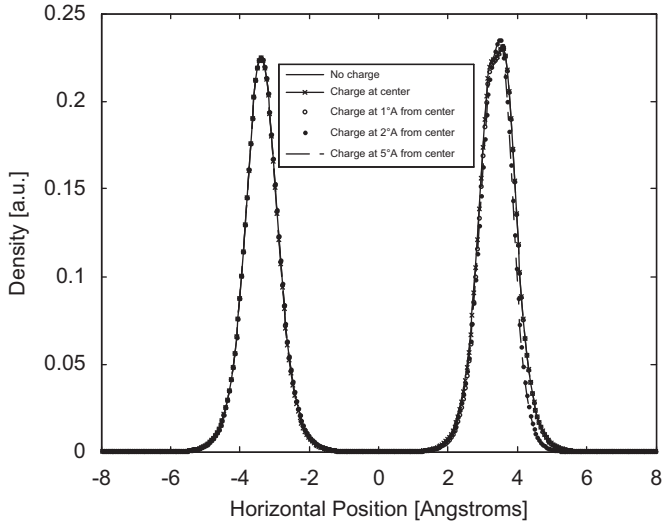

Fig. 10. Density profile along x1 direction.

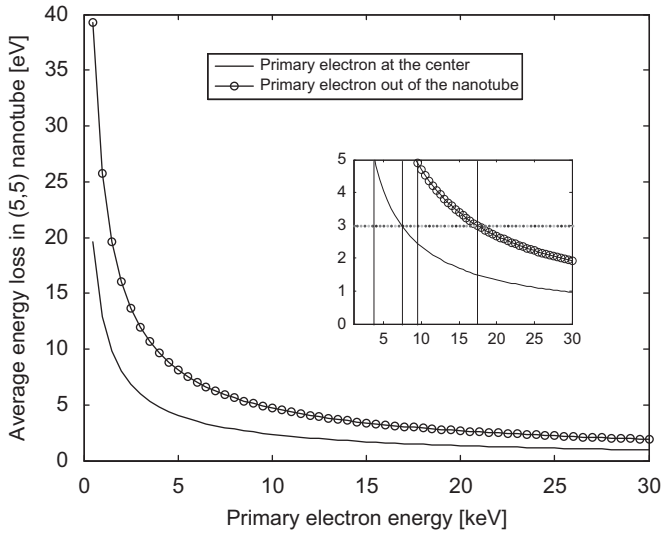

Fig. 11. Estimated average energy loss for different primary beam energies. Inset shows the primary beam energy limits for ~5 and ~3 eV energy loss.

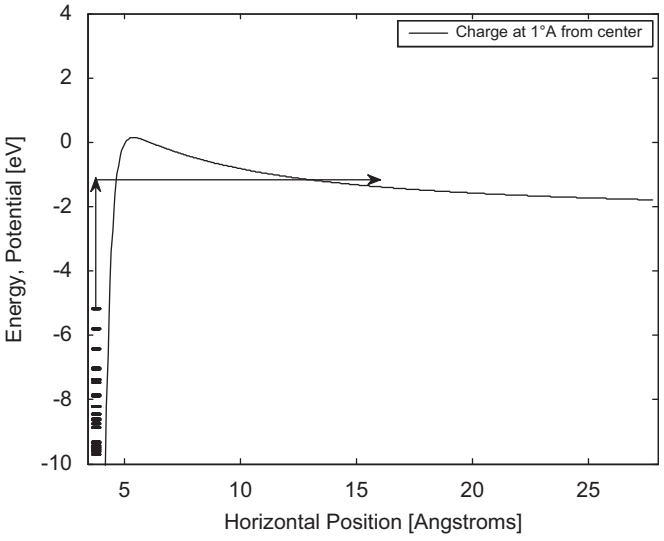

Fig. 12. Potential profile showing the probability of tunneling for charge at 1 Å from the center.

3.2. Effect of image potential on (5,5) SWNT

An important issue to be considered is the fact that once an electron (in this case a secondary electron) is emitted, its electric field will affect the distribution of the nanotube electrons and create a so-called image potential. This can affect the emission current. This effect has been studied in the context of field-emission in [23]. In order to investigate this effect for secondary emission, we placed a test charge (in addition to the primary electron) at various positions in different directions, namely at 5, 7 and 9 Å from the center of the tube in the x1, −x1 and −y1 directions. Assuming that the nanotube remains uncharged throughout the secondary emission process, it was seen that the resulting image potential leads to a further raise of the HOMO level (up to ∼3.5 eV depending upon the position of the secondary electron), that is a decrease in the effective potential barrier for secondary emission in certain directions. Fig. 13 shows this effect on the emission barrier in the x1 direction when the test charge is placed in the opposite side of the nanotube. Note, however, that this will not affect the fundamentals of the discussion presented in the earlier sections.

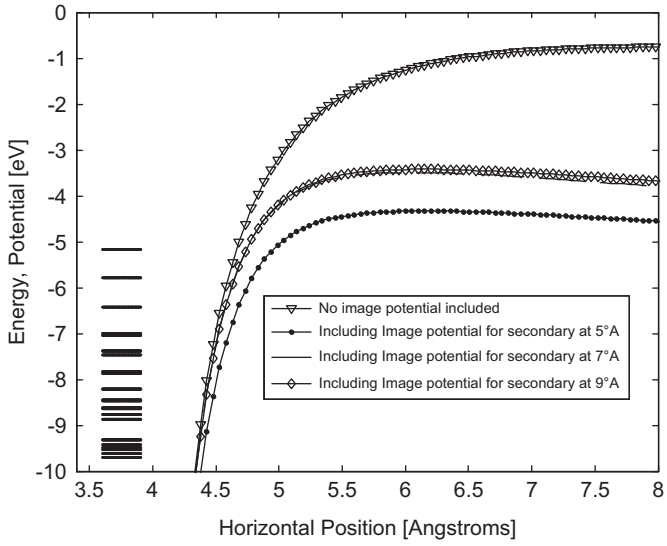

Fig. 13. Potential profile and energy levels of (5,5) SWNT showing the effect of image potential with primary electron at 2 Å from the center and secondary placed at 5, 7and 9 Å in −x1 direction.

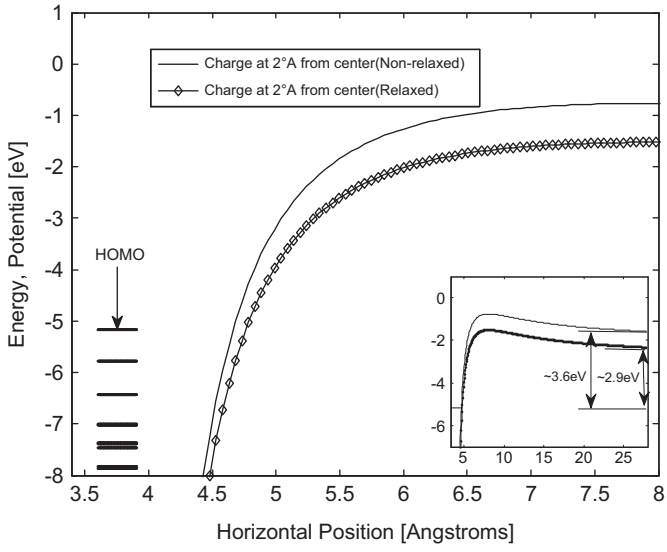

Fig. 14. Potential profile and energy levels of (5,5) SWNT showing the effect of relaxation with an electron at 2 Å from the center.

3.3. The relaxed (5,5) SWNT

In this section, the results are discussed for the case where the extra electron was fixed at various positions and a further geometry optimization was carried out before the single point energy calculation. The results were compared to that of the non-relaxed structure and Fig. 14 shows the most important case (when the charge was just inside the nanotube). It can be seen that when the nanotube structure itself is assumed to "respond" to the field of the incoming electron, the ionization energy is lowered by an additional ∼1 eV. Correspondingly, the probability of secondary emission is even higher according to the mechanisms discussed previously. In reality, it is likely that the nanotube will not have enough time to fully relax in the field of the incoming primary electron, and the situation is somewhere between the two extreme cases (non-relaxed and fully relaxed).

3.4. The (8,0) SWNT

The above simulations were also performed on an (8,0) SWNT. The results are not discussed in detail here since the general behaviors were very similar to those observed for the (5,5) SWNT. We expect less secondary emission from semiconducting nanotubes at higher scanning energies (> ∼7.5 keV) as more energy is needed for the HOMO–LUMO or other occupied–unoccupied state transitions than for the metallic nanotubes.

4. Summary

In summary, the effect of primary electrons on the electronic structure of carbon nanotubes was investigated using ab-initio simulations in order to gain insight into the mechanisms of secondary electron emission from nanotubes. The addition of an extra electron as a background charge particle to the system, mimicking the primary beam of a scanning electron microscope, causes an upward shift in the highest occupied molecular orbital (HOMO) and makes it easier for nanotube electrons to overcome the vacuum barrier or tunnel out. This effect is uniformly present regardless of where the extra electron is positioned, unless it is too far away (∼10 Å or more from the center of the nanotube). It was observed that primary electrons with lower energies (a few hundred eV to ∼10 keV) can transfer enough energy to the nanotube electrons to allow secondary emission. This is consistent with the fact that in experiments it is much easier to observe nanotubes at low primary beam energies. For primary electron energies of more than ∼10 keV, it seems unlikely that the energy transfer from one primary electron alone could lead to secondary emission. In such cases, either a multiple-step process or other mechanisms such as energy absorption by surface plasmons and subsequent transfer to other electrons to be emitted might be the root cause.

Acknowledgements

We acknowledge financial support from the Natural Sciences and Engineering Research Council (NSERC) of Canada. The simulations were performed using WestGrid high performance computing facility.

References

[1] P. Yaghoobi, A. Nojeh, Mod. Phys. Lett. B 21 (2007) 1807.
[2] S. Bandow, A.M. Rao, K.A. Williams, A. Thess, R.E. Smalley, P.C. Eklund, J. Phys. Chem. B 101 (1997) 8839.
[3] R. Andrews, D. Jacques, A.M. Rao, F. Derbyshire, D. Qian, X. Fan, E.C. Dickey, Chem. Phys. Lett. 303 (1999) 467.
[4] M. Terrones, F. Banhart, N. Grobert, J.-C. Charlier, H. Terrones, P.M. Ajayan, Phys. Rev. Lett. 89 (2002) 075505-1.
[5] A. Nojeh, W.K. Wong, E. Yieh, R.F. Pease, H. Dai, J. Vac. Sci. Technol. B. 22 (2004) 3124.
[6] A. Nojeh, B. Shan, K. Cho, R.F.W. Pease, Phys. Rev. Lett. 96 (2006) 056802-1.
[7] W.K. Wong, A. Nojeh, R.F.W. Pease, Scanning 28 (2006) 219.
[8] T. Brintlinger, Y.-F. Chen, T. Dürkop, E. Cobas, M.S. Fuhrer, Appl. Phys. Lett. 81 (2002) 2454.
[9] L.C. Qin, X. Zhao, K. Hirahara, Y. Ando, S. Iijima, Chem. Phys Lett. 349 (2001) 389.
[10] Y. Homma, S. Suzuki, Y. Kobayashi, M. Nagase, Appl. Phys. Lett. 84 (2004) 1750.
[11] P. Finnie, K. Kaminska, Y. Homma, D.G. Austing, J. Lefebvre, Nanotechnology 19 (2008) 335202-1.
[12] D.C. Joy, Monte Carlo Modeling for Electron Microscopy and Microanalysis, Oxford University Press, New York, 1995.
[13] C. Kim, B. Kim, S.M. Lee, C. Jo, Y.H. Lee, Phys. Rev. B 65 (2002) 165418-1.
[14] S. Han, M.H. Lee, J. Ihm, Phys. Rev. B 65 (2002) 085405-1.
[15] M.J. Frisch, et al., Gaussian 03, Revision C.02, Gaussian Inc., 2004.
[16] T. Mirfakhrai, R.K. Prasad, A. Nojeh, J.D.W. Madden, Nanotechnology 19 (2008) 315706-1.
[17] X. Zheng, G. Chen, Z. Li, S. Deng, N. Xu, Phys. Rev. Lett. 92 (2004) 106803-1.
[18] J. Peng, Z. Li, C. He, S. Deng, N. Xu, X. Zheng, G. Chen, Phys. Rev. B 72 (2005) 235106-1.
[19] R. Browning, T.Z. Li, B. Chui, Jun Ye, Z. Zeyzewski, D.C. Joy, J. Appl. Phys. 76 (1994) 2016.
[20] Z. Zeyzewski, D.O. MacCalium, A. Romig, D.C. Joy, J. Appl. Phys. 68 (1990) 3066.
[21] D.C. Joy, S. Luo, Scanning 11 (1989) 176.
[22] W.R. Leo, Techniques for Nuclear and Particle Physics Experiments: A How to Approach, 2nd revised ed., Springer, Berlin, 2005, pp. 24–25.
[23] W. Wang, J. Peng, G. Chen, S. Deng, N. Xu, Z. Li, J. Appl. Phys. 104 (2008) 034306-1.